Science Advances
AAAS

Supplementary Materials for

Functional imaging and quantification of multineuronal olfactory responses in *C. elegans*

Albert Lin *et al.*

Corresponding author: Albert Lin, albertlin@g.harvard.edu; Cengiz Pehlevan, cpehlevan@seas.harvard.edu; Mei Zhen, meizhen@lunenfeld.ca; Aravinthan D.T. Samuel, samuel@g.harvard.edu

Sci. Adv. **9**, eade1249 (2023)
DOI: 10.1126/sciadv.ade1249

This PDF file includes:

Supplement

Supplemental methods

A: Identifying neurons in the ZM10104 strain

The ZM10104 strain used in this experiment expresses two fluorescent proteins: GCaMP6s driven by the *ift-20* promoter, and wCherry driven by *gpc-1*. GCaMP6s expression was localized to neuronal nuclei to minimize spatial overlap of neighboring neurons, and to make identification of neurons easier. The promoter *ift-20* drives GCaMP expression in all ciliated sensory neurons. Our neurons of interest, the chemosensory neurons, lie in the lateral ganglia, but note that this promoter is pan-sensory, driving expression in cells outside of the lateral ganglia. The wCherry landmark is expressed in the cytoplasm of AFD, AWB, ASI, ASE, AWC, and ASJ. Note that it also is expressed in RIB, a neuron which is not labeled with GCaMP.

Relative positions are given in the orientation in **Figure S1**, with the nose to the left, the tail to the right, dorsal top, and ventral bottom. Relative positions should be interpreted as “usually but not always," unless otherwise noted. Also note that overly compressing an animal in any direction will distort the relative positions. Before identifying neurons, it is important to identify the orientation of the animal in the recording by figuring out where the dorsal-ventral (DV) plane lies. This is most easily done by identifying the plane of bilateral symmetry. Once you have oriented yourself, you can begin to identify neurons.

The easiest neurons to immediately identify in this strain are ASH, ASJ, and the anterior “triplet" of ASK, ADL, ASI. It is often effective to identify these neurons first, then work on the other neurons using the color landmarks and process of elimination. AWC and ASE should usually be in the neighborhood of ASH, and the four neurons AWA, AWB, ADF, and ASG are between ASH and the anterior triplet. These four neurons occasionally overlap. To avoid signal mixing, overlapping neurons were excluded from the dataset. For each odorant condition, neuronal identification was carried out independently by at least two individuals.

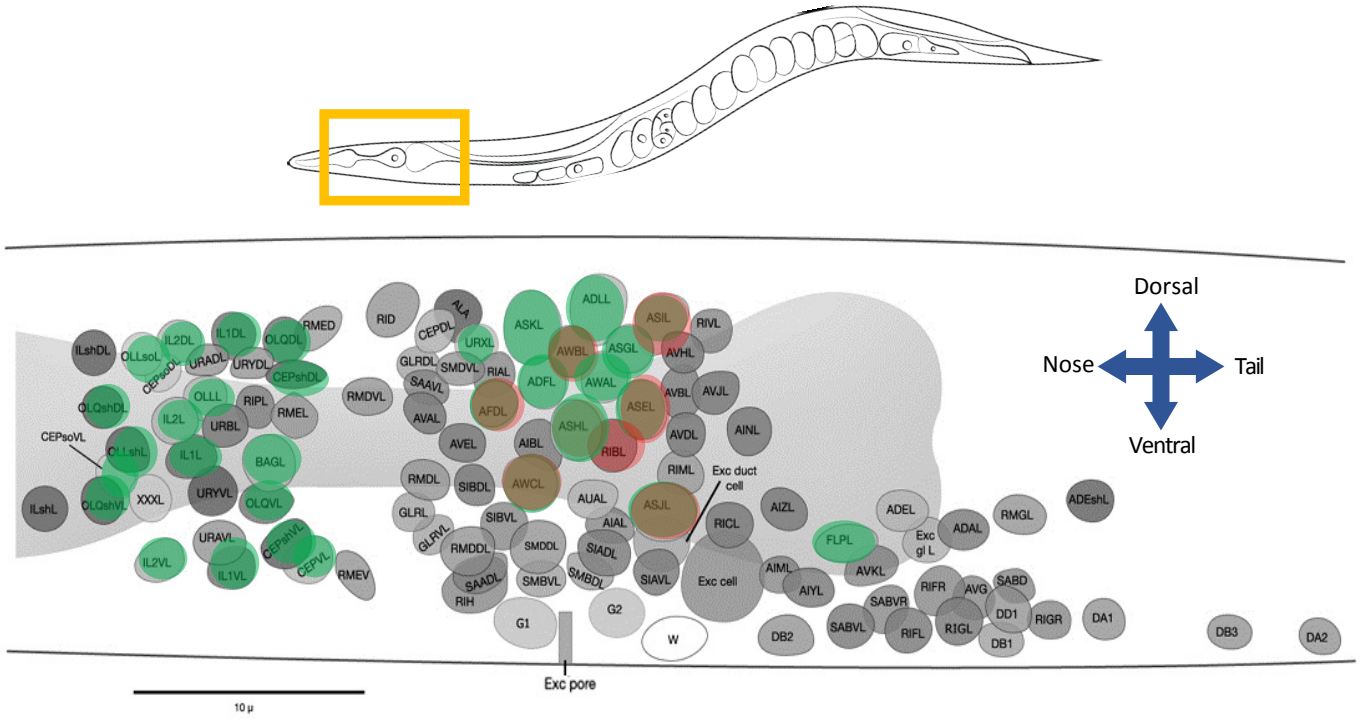

Figure S1. Identifying neurons in the ZM10104 strain. The *ift-20* promoter drives GCaMP expression in the nuclei of ciliated sensory neurons. The nuclei of the chemosensory neurons are all posterior to the nerve ring. A red landmark is provided by cytoplasmic expression of wCherry in the neurons AFD, AWB, ASI, ASE, AWC, and ASJ. Underlying *C. elegans* figure adapted from the digital version of White et al. 1986 (Wormbook)(50).

Table S1: Criteria for identifying each neuron class

Neuron	Color(s)	Relative Position	Notes
ASK	green	leftmost of the anterior triplet	large. do not confuse with URX, a small oblong neuron above ASK
ADL	green	part of the anterior triplet	larger than ASI
ASI	green & red	part of the anterior triplet	use color to distinguish from ADL
ASH	green & red	left of ASE, below AWA	bright, circular
ASE	green & red	right of ASH	smaller than ASH
AWC	green & red	variable. below ASH but can be to the left, directly below, or to the right	often oblong in shape
ASJ	green & red	tail end of the ganglion, bottom left	distance from AWC can vary
AWA	green	variable. usually above ASH	smaller than ASH, circular
AWB	green & red	position variable, usually directly below the anterior triplet	small, dim, a bit oblong. use color to identify
ADF	green	usually left of AWA, AWB	dim
ASG	green	usually right of AWA, AWB	small, circular

To minimize the chances of incorrect identification, neuronal IDs for each odorant condition were reviewed by at least two individuals, and ambiguous neurons were omitted from the analyzed datasets.

B: Olfactory stimuli and behavioral valences

Table S2: List of odorants

Odorant	Chemical class	Behavioral valence (low conc.)
1-pentanol	alcohol	attractive
1-hexanol	alcohol	attractive
1-heptanol	alcohol	repulsive
1-octanol	alcohol	repulsive
1-nonanol	alcohol	repulsive
isoamyl alcohol	alcohol	attractive
geraniol	alcohol	attractive
benzaldehyde	aromatic	attractive
methyl salicylate	aromatic	attractive
ethyl acetate	ester	attractive
ethyl butyrate	ester	attractive
ethyl heptanoate	ester	attractive
pentyl acetate	ester	attractive
butyl butyrate	ester	attractive
diacetyl	ketone	attractive
2-butanone	ketone	attractive
2-heptanone	ketone	attractive
2-nonanone	ketone	repulsive
2,3-pentanedione	ketone	attractive
2,5-dimethylpyrazine	pyrazine	attractive
2-methylpyrazine	pyrazine	attractive
2-isobutylthiazole	thiazole	attractive
2,4,5-trimethylthiazole	thiazole	attractive

C: Neuron tracking and signal extraction

To segment the neuronal nuclei in each recording, we built a GUI which allows users to navigate each 3D landmark image and click to add or remove neuron centers (21, 74). This GUI allows the user to toggle between multiple fluorescent channels and a maximum projection, allowing the user to take advantage of any fluorescent landmark labels in the strain. Complete labeling of all neuron centers is only necessary once for a given animal, even if multiple recordings have been made. The user then labels a small handful of widely spaced neurons (4-8) in the first frame of the activity recording. This small number of labeled neurons helps the tracking algorithm to compensate for any global motion or distortion that may have occurred in the animal between the landmark volume and the activity movie. In addition to segmentation, the GUI allows neurons to be manually identified. The names the user applies are then associated with the activity traces of those neurons.

Neighborhood correlation tracking of individual neurons

While the entire brain of the worm can distort substantially across large distances, the neighborhood immediately surrounding a neuronal nucleus of interest tends to remain consistent, with little local deformation. Our image registration strategy relies on this fact. Instead of attempting to identify neuron centers in every frame, we try to match the neighborhood surrounding the neuron center in the first frame to the most similar neighborhood in the following frame. We then return the center of the new neighborhood as the position of the neuron center in the next frame.

We first employ this approach to map the neuron centers identified in the high-resolution landmark volume during the segmentation step onto the first frame of the activity movie, which is captured at a lower resolution. We then proceed to compare each frame of the movie to the next. The neighborhood correlation comparison is made independently for each neuron. While we lose some information about local deformations by not integrating information about how neighboring neurons are moving, we gain the ability to run the tracking of each neuron in a dataset as a parallel process, dramatically decreasing runtime. This also prevents a mistake in tracking one neuron from propagating to other nearby neurons. We run the tracking on a down-sampled version of the activity movie, also to improve runtime.

For a given neuron center, the tracking algorithm goes through the following steps:

1. Given the position of the given neuron center in the current frame, $n_t = (x_t, y_t, z_t)$, we identify the neuron's local 3D neighborhood N_t in that frame, the volume with dimensions $2a * 2b * 2c$, in the region spanned by $[x_t - a, x_t + a]$, $[y_t - b, y_t + b]$, and $[z_t - c, z_t + c]$.

2. We identify the naive center in frame $t+1$, from where we begin our search for the neighborhood most similar to N_t. For the first frame of the movie, this point is adjusted by a distance-weighted average of the manually labeled neurons: $n'_{t+1} = (x_t + \Delta\Sigma w x^i, y_t + \Delta\Sigma w y^i, z_t + \Delta\Sigma w z^i)$. For any other frame, we simply take the naive center as the center of the previous frame, $n'_{t+1} = n_t = (x_t, y_t, z_t)$.

3. Starting from the naive center n'_{t+1}, we perform image registration between the maximum intensity projections in x, y, and z of putative neighborhood N'_{t+1} and the previous neighborhood N_t, computing the pairwise correlation of these images. We then repeat this process, moving the putative center n'_{t+1} by 1 pixel per iteration until one of the following occurs:

   (a) The algorithm finds a putative neighborhood N'_{t+1} whose correlation with N_t exceeds the confidence threshold C (usually set at above 90%). This putative neighborhood is then defined as N_{t+1}.

   (b) The algorithm tests all putative neighborhoods within a maximum search radius $r_{\max}$ of the naive center n'_{t+1}, but failed to find a putative neighborhood whose correlation exceeds the confidence threshold C. The algorithm then returns the putative neighborhood with the highest correlation with N_t as N_{t+1}.

   (c) If no neighborhood is found with a correlation exceeding a minimum value, the neuron is considered lost in frame $t+1$, likely either due to motion taking the neuron outside the region of interest. No center is reported, and the last reported neighborhood N_t is used as the basis of comparison for following frames ($t+2, t+3$, etc.).

4. The center of neighborhood N_{t+1} is defined as the neuron center in this frame, n_{t+1}.

5. Repeat until the end of the activity movie is reached.

We can optimize the tracking parameters such as neighborhood size (a, b, c), maximum search radius $r_{\max}$, and confidence threshold C for both accuracy and speed for different imaging conditions.

Extracting calcium dynamics

To extract calcium signals, we first map the positions of each tracked neuron center back onto the original-resolution volumetric images. We then extract fluorescence values from these images. We identify a small volume around each neuron center, containing voxels whose fluorescence will be assigned to the neuron. This volume is set as 2 µm x 2 µm x 3 µm for our data. We compute the mean of the 10 brightest pixels within this volume to extract a raw fluorescence trace $F_r(t)$. We then account for photobleaching by exponential detrending, giving us a clean fluorescence activity trace $F(t)$. We then identify the background fluorescence F_0 for each neuron, and report normalized neuron activity $\Delta F/F_0$.

Manual proofreading of traces

Manual proofreading is an opportunity to improve data quality by removing neurons which have been mistracked, adjusting the computer-determined baseline fluorescence F_0, and correcting or adding nuclear IDs. Proofreading also enabled us to remove traces which were contaminated by signals from neighboring neurons. The software then compiles all processed traces for a given individual into a single data structure.

D: Imputing missing single-trial responses

Across trials of all neurons and all conditions, about 20% of the neuron responses were either not captured, or excluded due to tracking mistakes or signal contamination issues. To perform single-trial discrimination analysis in the (N-dimensional) neural response space, we first had to fill these missing data points in a reasonable and biologically motivated way.

For a given odorant and M trials, the peak responses of the $N = 11$ sensory neurons can be compiled in a matrix $R \in \mathbb{R}^{N \times M}$. Without any assumptions for the values R, it is impossible to infer the missing data. Fortunately, due to the intrinsic correlation between the responses of different olfactory neurons, the full response matrix R is low rank (as indicated by the PCA of neural responses). We can use this low-rank information to recover the missing entries: "matrix completion" algorithms can solve this problem very efficiently (77, 78).

To verify that matrix completion can indeed recover the missing entries faithfully, we performed a holdout evaluation. For the response matrix to each odor, we performed matrix completion after randomly removing 20 entries ($x_i, i = 1, \cdots, 20$). The imputed matrix is denoted as X^*. We then calculated the Pearson correlation coefficient ρ between the estimated entries x_i^* with the true entries x_i. The average value of ρ is around 0.7 (**Figure S6A-B**). We used the MATLAB code provided in (79) with default parameters for matrix completion (`https://github.com/udellgroup/Codes-of-FGSR-for-effecient-low-rank-matrix-recovery`). Specifically, we chose an algorithm based on minimization of the nuclear norm `MC_Nulcear_IALM`.

E: Computational methods for discriminability quantification

For binary classification of all odorant pairs, we used linear regression and a simple SVM (linear or Gaussian kernel). To decode odor identity from the entire single-trial dataset, we built a multi-class classifier. We concatenate all of the single-trial responses of the 23 odorants at high concentration. Each trial is an 11-dimensional point, one dimension for every neuron class. Each point has an associated label indicating the odorant identity. This data set was randomly divided into 10 parts, 9 of which are used as a training set (90%) and one which is used as a validation set (10%).

We used the MATLAB function `fitcecoc` to fit a multi-class model which supports both SVM and other classifiers. Mechanistically, this method reduces the problem of overall classification into a sequence of binary classification problems. The performance was quantified by the classification error, estimated using the `crossval` function. The confusion matrix was generated using the functions `kfoldPredict` and `confusionchart`. The training is repeated 10 times, using each of the 10 parts of the datasets as the validation set, and the results were compiled.

For the *in silico* knockouts, we removed neurons from the training dataset, resulting, for example in 10-dimensional responses when one neuron was removed. We trained the multi-class classifier as above.

F: Statistics, code, and software

All statistical computations and image analysis code were written and run in MATLAB using standard toolboxes, with the exception of the OME Bio-Formats API (used to read Nikon ND2 file formats) (80) and CET Perceptually Uniform Color Maps (81).

Supplemental figures

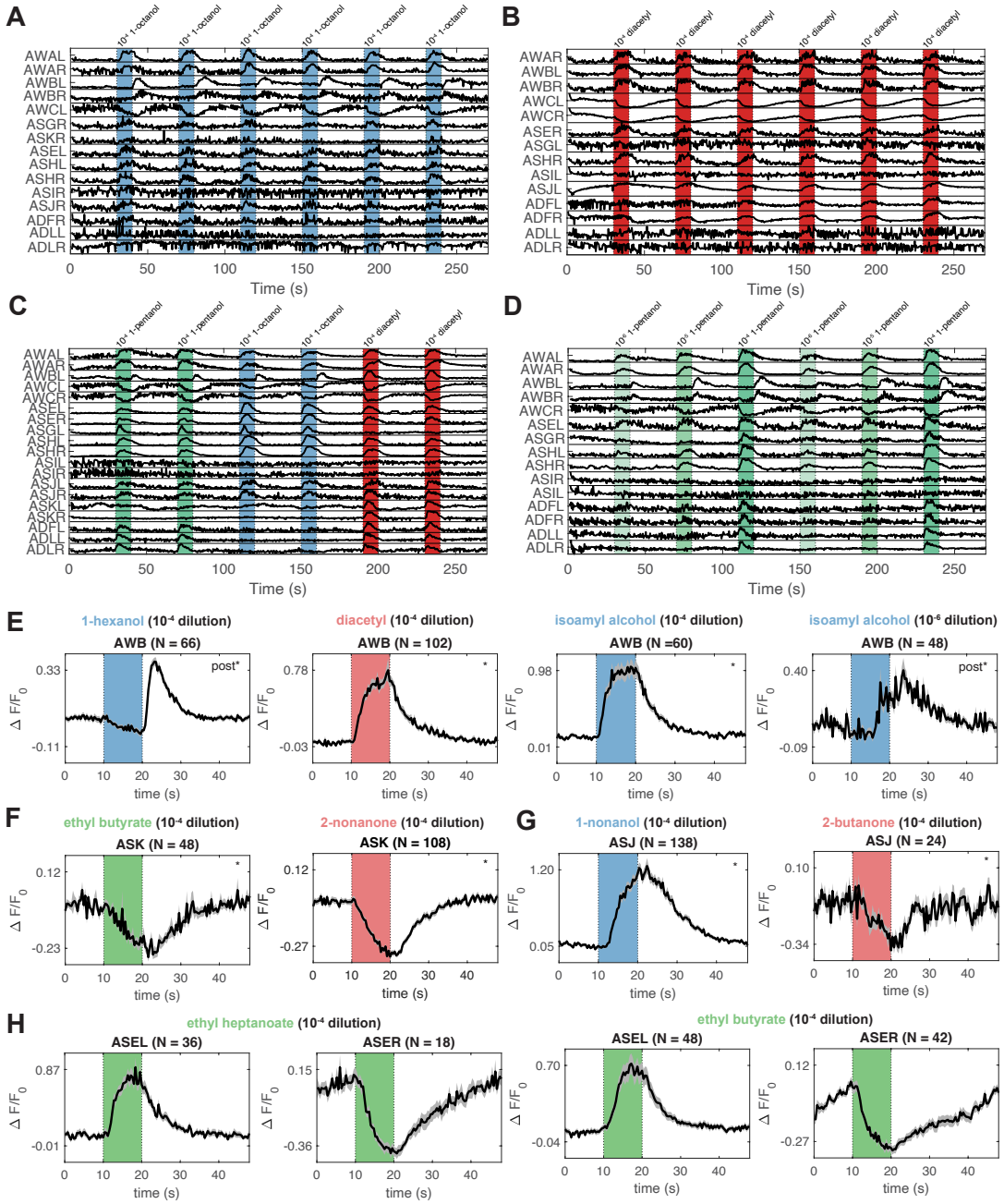

Figure S2. Single neuron response observations and example experiments. Examples of single experiments in which an animal was presented with multiple pulses of **(A)** 1-octanol and **(B)** diacetyl at the same concentration, demonstrating the consistency of sensory neuron responses under these conditions. Note that in each experiment, some neurons are missing due to occlusion or signal contamination. **(C)** A control experiment in which three odorants were presented to a single animal, evoking distinct and reproducible responses. **(D)** A control experiment in which one odorant (1-pentanol) was presented at 3 concentrations, evoking distinct and reproducible responses at each concentration. **(E)** AWB is an OFF response for most stimuli, such as 1-hexanol, but is occasionally an ON response, as is the case for high concentration diacetyl. High concentration isoamyl alcohol elicits an ON response from AWB, but low concentration isoamyl alcohol elicits an OFF response. This has been previously observed in Yoshida et al., 2012 (15). **(F)** We observe inhibitory responses to some odorants in ASK. **(G)** ASJ has an excitatory response to some odorants, such as 1-nonanol, but has an inhibitory response to 2-butanone. **(H)** We observe L/R asymmetries in ASE in response to several odorants, such as ethyl heptanoate and butyl butyrate.

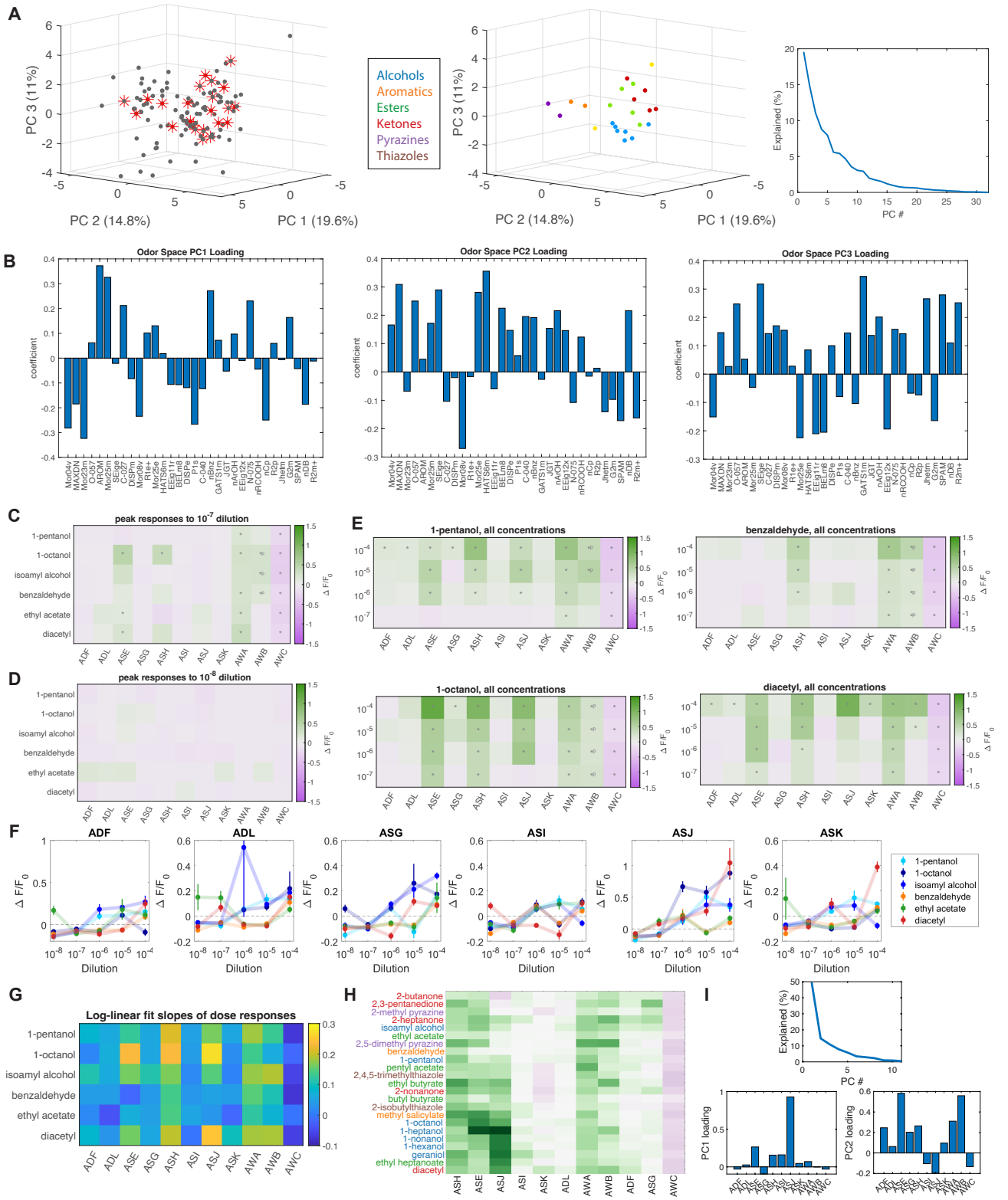

Figure S3. Supplemental panels for Figure 2. (A) An odor space constructed from the molecular descriptors of 122 odorants (gray) previously studied in *C. elegans*. We selected for our experiments a panel of 23 odorants (red) which span the odor space (left). These 23 odorants are presented in odor space colored by their chemical class (center). On the right is the variance explained as a function of the PC number in the odor space. **(B)** The molecular descriptor loadings of the first 3 principal components of the *C. elegans* odor space, plotted on the same axes. The leading components of PC 1 are measures of aromaticity, and the leading components of PC2 are measures of electronegativity. Peak responses for six odors tested at **(C)** 10^{-7} and **(D)** 10^{-8} dilutions. Statistically significant responses ($q \leq 0.01$) are indicated with stars—no significant activity was observed at the lowest tested dilution. **(E)** Compiled responses to three representative odorants at multiple concentrations (1-pentanol, 1-nonanol, and benzaldehyde) show similar neural responses across concentration. The magnitude of neuron responses generally increases with increasing concentration, and for some conditions, additional neurons are recruited at high concentration. **(F)** Dose responses for the six sensory neurons not printed in **Figure 2E**. **(G)** The fitted log-linear slopes m for the dose response of each neuron-odorant pair. The peak responses r as a function of odorant dilution c were fitted to the equation $r(c) \approx m \log_{10} c + I$, and the slope m was determined through linear regression. **(H)** Odorants (high concentration) clustered by their peak average neuronal responses. **(I)** The variance explained and the loadings of the first two principal components of the standardized average peak neural response PC space in **Figure 2F**.

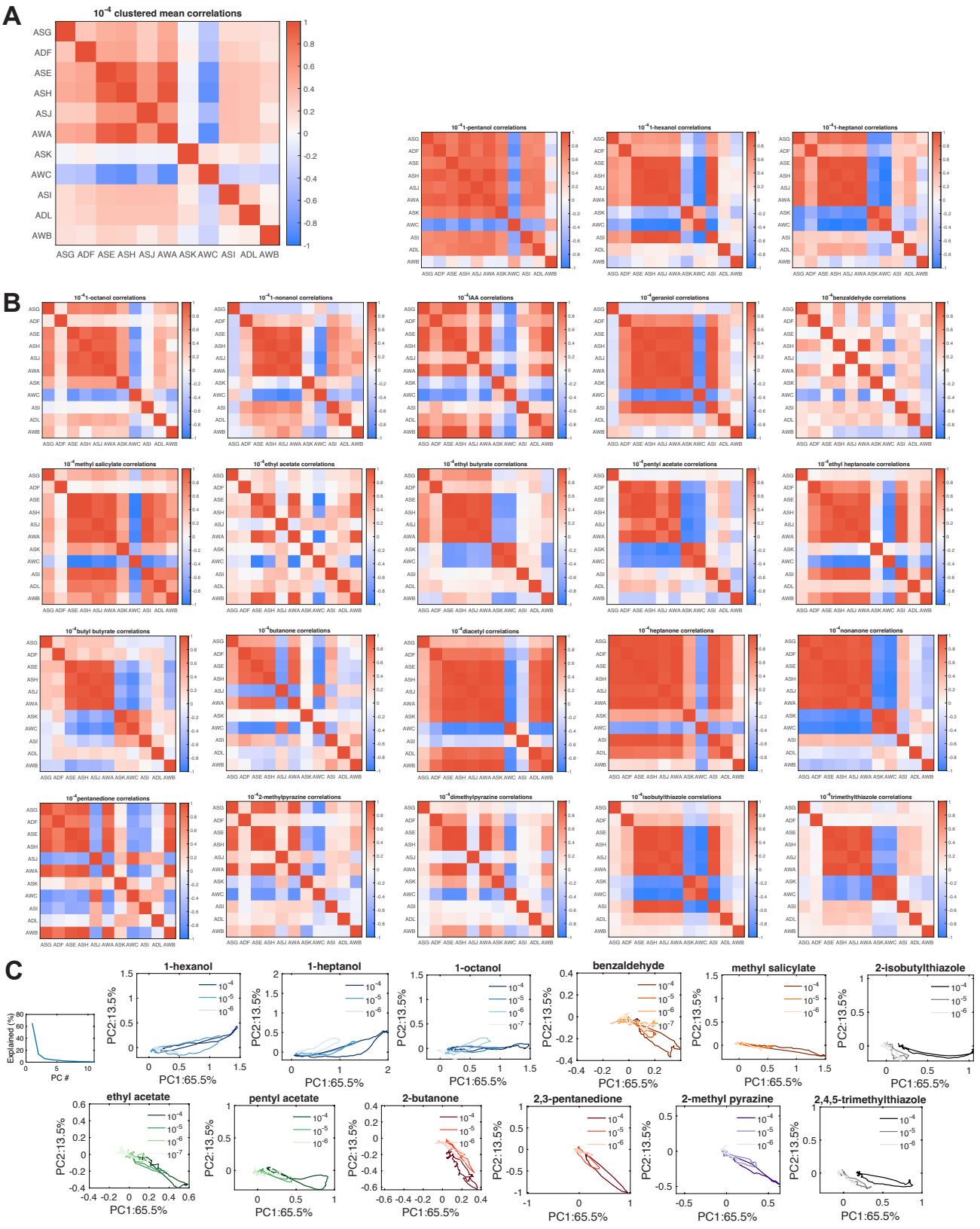

Figure S4. Time trace correlations and phase trajectory analyses. (A) Average time trace correlation map of the 11 chemosensory neuron responses across all 23 odorants. **(B)** Average correlation maps of responses to all 23 odorants at high concentration, plotted on the same axes, show diverse response dynamics. **(C)** Phase trajectory plots of average neural activity for select odorants, all plotted in a common PC space (Pareto plot of the PC space on the left). The shade of each color indicates concentration, with low concentration indicated by a light shade and high concentration indicated by a dark shade. Different concentrations of the same odorant tend to generate similar trajectories.

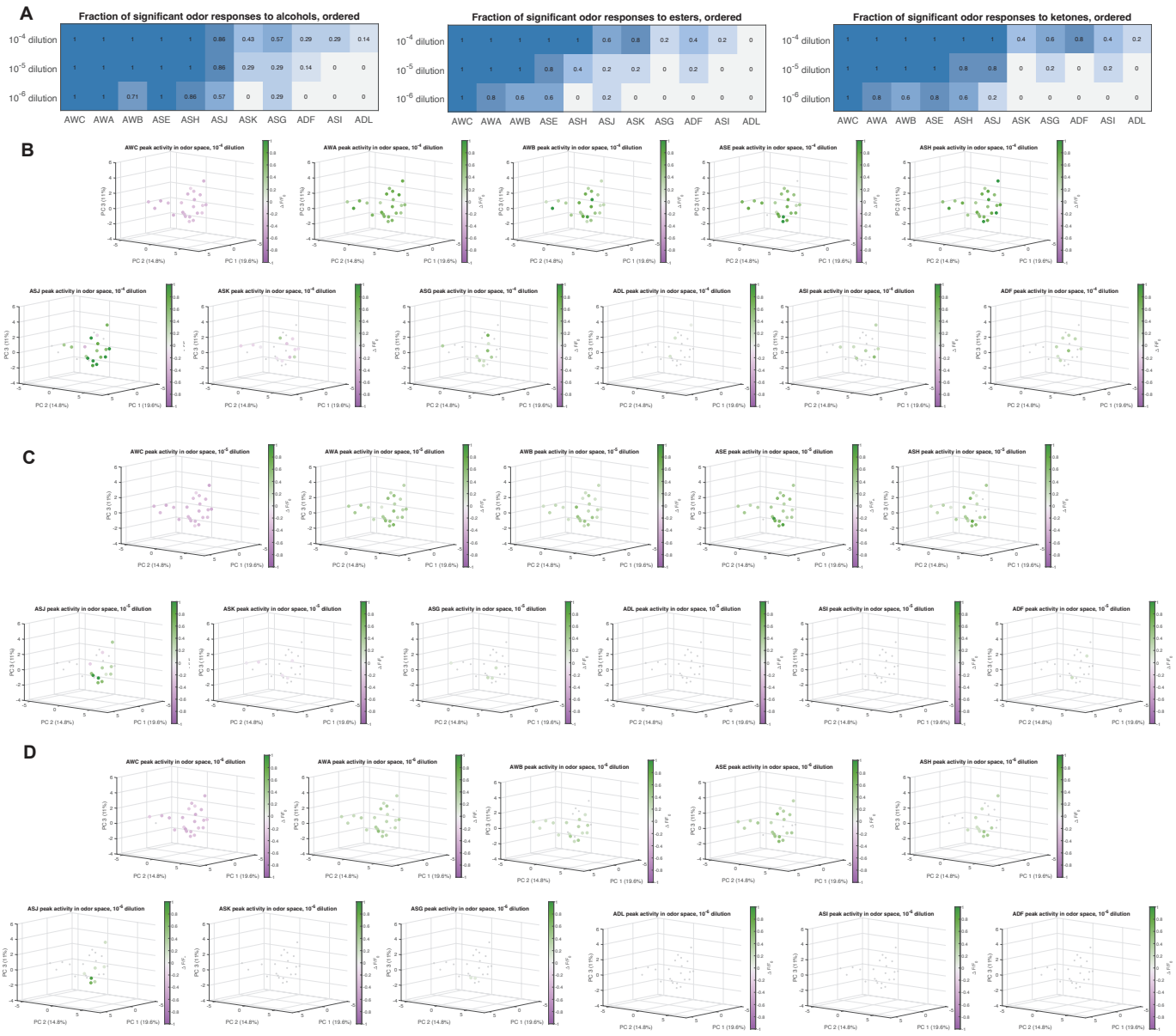

Figure S5. Average peak responses plotted in odor space. (A) The fraction of significant odor responses to three chemical groups: alcohols (7 total stimuli), esters (5 total stimuli), and ketones (5 total stimuli). Neurons are ordered by overall response fraction (**Figure 4A**). Average peak responses of each of the 11 chemosensory neuron classes plotted in odor space (**Figure S3A**), at **(B)** high odorant concentration (10^{-4}), **(C)** medium odorant concentration (10^{-5}), and **(D)** low odorant concentration (10^{-6}).

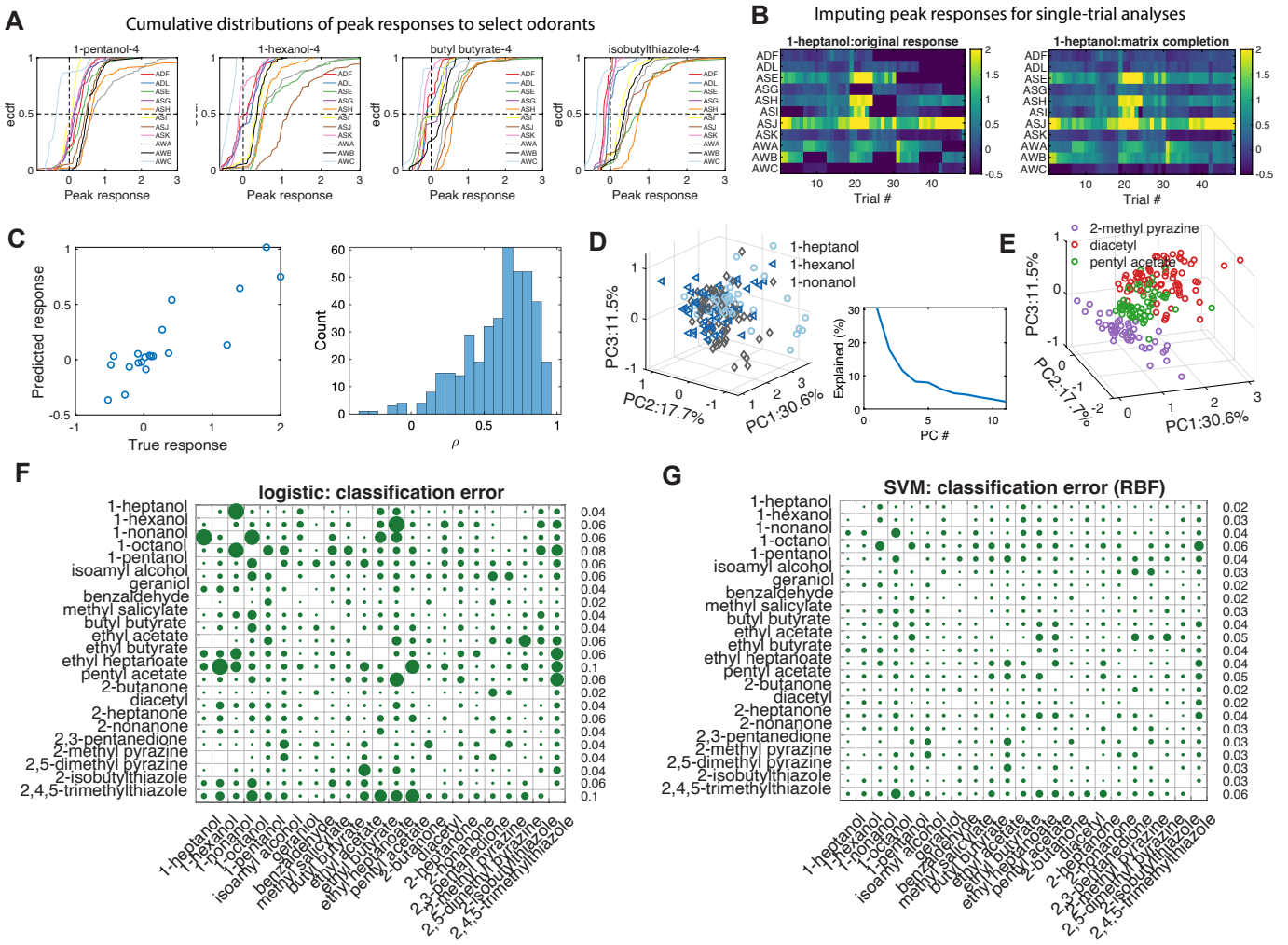

Figure S6. Supplemental panels for Figure 5. (A) Cumulative distributions of peak responses of every neuron (four exemplar odorants shown). **(B)** Signals were not always captured from all 22 chemosensory neurons in every trial. We used a matrix completion algorithm to impute these missing data points. Here are shown the peak responses all chemosensory neurons to 1-heptanol in different trials, with missing responses in dark blue (left) and after matrix completion (right). **(C)** *Left*: To quantify the performance matrix completion, we randomly removed 20 measured responses (true response) and compared the imputed values from matrix completion (predicted responses).*Right*: The histogram of Pearson's correlation coefficient between true responses and predicted responses. For each response matrix, we repeated 5 times. **(D/E)** Representations of single-trial peak neural responses to sets of **(D)** three similar and **(E)** three dissimilar odorants. These data are plotted in a PC space constructed from the individual trial responses to all odorants in the dataset. (Inset: The Pareto plot of the variance explained by each PC.) **(D)** We see that three similar odorants, the straight-chain alcohols 1-hexanol, 1-heptanol, and 1-nonanol, have more similar neural representations. **(E)** In contrast, three odorants of three distinct chemical classes, 2-methylpyrazine (a pyrazine), diacetyl (a ketone), and pentyl acetate (an ester), have more easily separable neural representations. Binary classification of all odorant pairs by **(F)** logistic regression and **(G)** SVM. Both methods return very low classification errors, demonstrating that the single-trial peak responses of any two odorants can be distinguished. Shown here are classification error heatmaps at high concentration (10^{-4} dilution), for which the average classification error is 0.055 for the logistic regression and 0.035 for the SVM.

REFERENCES AND NOTES

1. B. Malnic, J. Hirono, T. Sato, L. B. Buck, Combinatorial receptor codes for odors. *Cell* **96**, 713–723 (1999).

2. K. Nara, L. R. Saraiva, X. Ye, L. B. Buck, A large-scale analysis of odor coding in the olfactory epithelium. *J. Neurosci.* **31**, 9179–9191 (2011).

3. S. A. Kreher, D. Mathew, J. Kim, J. R. Carlson, Translation of sensory input into behavioral output via an olfactory system. *Neuron* **59**, 110–124 (2008).

4. G. Si, Jessleen K. Kanwal, Y. Hu, C. J. Tabone, J. Baron, M. Berck, G. Vignoud, A. D. T. Samuel, Structured odorant response patterns across a complete olfactory receptor neuron population. *Neuron* **101**, 950–962.e7 (2019).

5. J. W. Wang, A. M. Wong, J. Flores, L. B. Vosshall, R. Axel, Two-photon calcium imaging reveals an odor-evoked map of activity in the fly brain. *Cell* **112**, 271–282 (2003).

6. E. A. Hallem, J. R. Carlson, Coding of odors by a receptor repertoire. *Cell* **125**, 143–160 (2006).

7. J. del Marmol, M. A. Yedlin, V. Ruta, The structural basis of odorant recognition in insect olfactory receptors. *Nature* **597**, 126–131 2021.

8. M. De Bruyne, T. C. Baker, Odor detection in insects: Volatile codes. *J. Chem. Ecol.* **34**, 882–897 (2008).

9. P. S. Grewal, D. J. Wright, Migration of *Caenorhabditis elegans* larvae towards bacteria and the nature of the bacterial stimulus. *Fundam. Appl. Nematol.* **15**, 159–166 (1992).

10. C. I. Bargmann, H. Robert Horvitz, Chemosensory neurons with overlapping functions direct chemotaxis to multiple chemicals in *C. elegans*. *Neuron* **7**, 729–742 (1991).

11. C. I. Bargmann, Comparative chemosensation from receptors to ecology. *Nature* **444**, 295–301 (2006).

12. C. I. Bargmann, Chemosensation in *C. elegans*, *WormBook: The Online Review of C. elegans Biology* (2006), pp. 1–29; 10.1895/wormbook.1.123.1.

13. B. Vidal, U. Aghayeva, H. Sun, C. Wang, L. Glenwinkel, E. A. Bayer, O. Hobert, An atlas of *Caenorhabditis elegans* chemoreceptor expression. *PLOS Biol.* **16**, 1–34 (2018).

14. L. A. Perkins, E. M. Hedgecock, J. N. Thomson, J. G. Culotti, Mutant sensory cilia in the nematode *Caenorhabditis elegans*. *Dev. Biol.* **117**, 456–487 (1986).

15. K. Yoshida, T. Hirotsu, T. Tagawa, S. Oda, T. Wakabayashi, Y. Iino, T. Ishihara, Odour concentration-dependent olfactory preference change in *C. elegans*. *Nat. Commun.* **3**, 739 (2012).

16. J. Larsch, D. Ventimiglia, C. I. Bargmann, D. R. Albrecht, High-throughput imaging of neuronal activity in *Caenorhabditis elegans*. *Proc. Natl. Acad. Sci. U.S.A.* **110**, E4266–E4273 (2013).

17. S. G. Leinwand, C. J. Yang, D. Bazopoulou, N. Chronis, J. Srinivasan, S. H. Chalasani, Circuit mechanisms encoding odors and driving aging-associated behavioral declines in *Caenorhabditis elegans*. *eLife* **4**, e10181 (2015).

18. A. Zaslaver, I. Liani, O. Shtangel, S. Ginzburg, L. Yee, P. W. Sternberg, Hierarchical sparse coding in the sensory system of *Caenorhabditis elegans*. *Proc. Natl. Acad. Sci. U.S.A.* **112**, 1185–1189 (2015).

19. S. Yu, L. Avery, E. Baude, D. L. Garbers, Guanylyl cyclase expression in specific sensory neurons: A new family of chemosensory receptors. *Proc. Natl. Acad. Sci. U. S. A.* **94**, 3384–3387, (1997).

20. P. D. Wes, C. I. Bargmann, *C. elegans* odour discrimination requires asymmetric diversity in olfactory neurons. *Nature* **410**, 698–701 (2001).

21. E. Yemini, A. Lin, A. Nejatbakhsh, E. Varol, R. Sun, G. E. Mena, A. D. T. Samuel, L. Paninski, V. Venkatachalam, O. Hobert, NeuroPAL: A multicolor atlas for whole-brain neuronal identification in *C. elegans*. *Cell* **184**, 272–288–288.e11 (2021).

22. T. R. Thiele, S. Faumont, S. R. Lockery, The neural network for chemotaxis to tastants in *Caenorhabditis elegans* is specialized for temporal differentiation. *J. Neurosci.* **23**, 11904–11911 (2005).

23. H. Suzuki, T. R. Thiele, S. Faumont, M. Ezcurra, S. R. Lockery, and W. R. Schafer, Functional asymmetry in *Caenorhabditis elegans* taste neurons and its computational role in chemotaxis. *Nature* **454**, 114–117 (2008).

24. E. Z. MacOsko, N. Pokala, E. H. Feinberg, S. H. Chalasani, R. A. Butcher, J. Clardy, C. I. Bargmann, A hub-and-spoke circuit drives pheromone attraction and social behaviour in *C. elegans*. *Nature* **458**, 1171–1175 (2009).

25. A. Narayan, V. Venkatachalam, O. Durak, D. K. Reilly, N. Bose, F. C. Schroeder, A. D. T. Samuel, J. Srinivasan, P. W. Sternberg, Contrasting responses within a single neuron class enable sex-specific attraction in *Caenorhabditis elegans*. *Proc. Natl. Acad. Sci. U.S.A.* **113**, E1392–E1401 (2016).

26. J. S. Greene, M. Brown, M. Dobosiewicz, I. G. Ishida, E. Z. Macosko, X. Zhang, R. A. Butcher, D. J. Cline, P. T. McGrath, C. I. Bargmann, Balancing selection shapes density-dependent foraging behaviour. *Nature* **539**, 254–258 (2016).

27. E. Z. Aprison, I. Ruvinsky, Counteracting ascarosides act through distinct neurons to determine the sexual identity of *C. elegans* pheromones. *Curr. Biol.* 2589–2599.e3 **27**, (2017).

28. K. A. Fagan, J. Luo, R. C. Lagoy, F. C. Schroeder, D. R. Albrecht, D. S. Portman, A single-neuron chemosensory switch determines the valence of a sexually dimorphic sensory behavior. *Curr. Biol.* **28**, 902–914.e5 (2018).

29. P. T. McGrath, I. Ruvinsky, A primer on pheromone signaling in *Caenorhabditis elegans* for systems *biologists. Curr. Opin. Syst. Biol.* **13**, 23–30 (2019).

30. M. A. Hilliard, C. I. Bargmann, P. Bazzicalupo, *C. elegans* responds to chemical repellents by integrating sensory inputs from the head and the tail. *Curr. Biol.* **12**, 730–734 (2002).

31. M. A. Hilliard, C. Bergamasco, S. Arbucci, R. H. A. Plasterk, P. Bazzicalupo, Worms taste bitter: ASH neurons, QUI-1, GPA-3 and ODR-3 mediate quinine avoidance in *Caenorhabditis elegans*. *EMBO J.* **23**, 1101–1111 (2004).

32. J. M. Kaplan, H. R. Horvitz, A dual mechanosensory and chemosensory neuron in *Caenorhabditis elegans*. *Proc. Natl. Acad. Sci. U.S.A.* **90**, 2227–2231 (1993).

33. Y. Sambongi, T. Nagae, Y. Liu, T. Yoshimizu, K. Takeda, Y. Wada, M. Futai, Sensing of cadmium and copper ions by externally exposed ADL, ASE, and ASH neurons elicits avoidance response in *Caenorhabditis elegans*. *Neuroreport* **10**, 753–757 (1999).

34. A. Metaxakis, D. Petratou, N. Tavernarakis, Multimodal sensory processing in *Caenorhabditis elegans*. *Open Biol.* **8**, (2018).

35. C. I. Bargmann, E. Hartwieg, H. R. Horvitz, Odorant-selective genes and neurons mediate olfaction in *C. elegans*. *Neuron* **74**, 515–527 (1993).

36. S. H. Chalasani, N. Chronis, M. Tsunozaki, J. M. Gray, D. Ramot, M. B. Goodman, C. I. Bargmann, Erratum: Dissecting a circuit for olfactory behaviour in *Caenorhabditis elegans*. *Nature* **451**, 63–70 (2008).

37. M. Tsunozaki, S. H. Chalasani, C. I. Bargmann, A behavioral switch: cgmp and pkc signaling in olfactory neurons reverses odor preference in *C. elegans*. *Neuron* **59**, 959–971 (2008).

38. E. R. Troemel, B. E. Kimmel, C. I. Bargmann, Reprogramming chemotaxis responses: Sensory neurons define olfactory preferences in *C. elegans*. *Cell* **91**, 161–169 (1997).

39. Heon-ick Ha, M. Hendricks, Y. Shen, C. V. Gabel, C. Fang-Yen, Y. Qin, D. Colón-Ramos, K. Shen, A. D. T. Samuel, Y. Zhang, Functional organization of a neural network for aversive olfactory learning in *Caenorhabditis elegans*. *Neuron* **68**, 1173–1186 (2010).

40. D. Cheng, J. S. Lee, M. Brown, M. S. Ebert, P. T. McGrath, M. Tomioka, Y. Iino, C. I. Bargmann, Insulin/igf signaling regulates presynaptic glutamate release in aversive olfactory learning. *Cell Rep.* **41**, 111685 (2022).

41. M. Dobosiewicz, Q. Liu, C. I. Bargmann, Reliability of an interneuron response depends on an integrated sensory state. *eLife* **8**, e50566 (2019).

42. H. A. Colbert, C. I. Bargmann, Odorant-specific adaptation pathways generate olfactory plasticity in *C. elegans*. *Neuron* **14**, 803–812 (1995).

43. N. D. L'Etoile, C. M. Coburn, J. Eastham, A. Kistler, G. Gallegos, C. I. Bargmann, The cyclic GMP-dependent protein kinase EGL-4 regulates olfactory adaptation in *C. elegans*. *Neuron* **36**, 1079–1089 (2002).

44. G. Jansen, D. Weinkove, R. H. A. Plasterk, The G-protein γ subunit gpc-1 of the nematode *C. elegans* is involved in taste adaptation. *EMBO J.* **21**, 986–994 (2002).

45. M. A. Hilliard, A. J. Apicella, R. Kerr, H. Suzuki, P. Bazzicalupo, W. R. Schafer, In vivo imaging of *C. elegans* ASH neurons: Cellular response and adaptation to chemical repellents. *EMBO J.* **24**, 63–72 (2005).

46. S. Levy, C. I. Bargmann, An adaptive-threshold mechanism for odor sensation and animal navigation. *Neuron* **105**, 534–548.e13 (2020).

47. M. Khan, A. H. Hartmann, M. P. O'Donnell, M. Piccione, A. Pandey, P.-H. Chao, N. D. Dwyer, C. I. Bargmann, P. Sengupta, Context-dependent reversal of odorant preference is driven by inversion of the response in a single sensory neuron type. *PLOS Biol.* **20**, e3001677 (2022).

48. Q. Liu, P. B. Kidd, M. Dobosiewicz, C. I. Bargmann, *C. elegans* AWA olfactory neurons fire calcium-mediated all-or-none action potentials. *Cell* **175**, 57–70.e17 (2018).

49. I. G McLachlan, T. S. Kramer, M. Dua, E. M. Diloreto, U. Dag, J. Srinivasan, S. W. Flavell, Diverse states and stimuli tune olfactory receptor expression levels to modulate food-seeking behavior. bioRxiv 2022.04.27.489714 [**Preprint**]. 28 April 2022. https://doi.org/10.1101/2022.04.27.489714.

50. N. Chronis, M. Zimmer, C. I. Bargmann, Microfluidics for in vivo imaging of neuronal and behavioral activity in *Caenorhabditis elegans*. *Nat. Methods* **4**, 727–731 (2007).

51. S. E. Worthy, L. Haynes, M. Chambers, D. Bethune, E. Kan, K. Chung, R. Ota, C. J. Taylor, E. E. Glater, Identification of attractive odorants released by preferred bacterial food found in the natural habitats of *C. elegans*. *PLOS ONE* **13**, 1–14 (2018).

52. R. Haddad, R. Khan, Y. K. Takahashi, K. Mori, D. Harel, N. Sobel, A metric for odorant comparison. *Nat. Methods* **5**, 425–429 (2008).

53. P. Sengupta, J. H. Chou, C. I. Bargmann, odr-10 Encodes a seven transmembrane domain olfactory receptor required for responses to the odorant diacetyl. *Cell* **84**, 899–909 (1996).

54. P. J. Summers, R. M. Layne, A. C. Ortega, G. P. Harris, B. A. Bamber, R. W. Komuniecki, Multiple sensory inputs are extensively integrated to modulate nociception in *C. elegans*. *J. Neurosci.*, **35**, 10331–10342 (2015).

55. J. G. White, E. Southgate, J. N. Thomson, S. Brenner, The structure of the nervous system of the nematode *Caenorhabditis elegans*. *Philos. Trans. R. Soc. Lond. B Biol. Sci.* **314**, 1–340 (1986).

56. D. Witvliet, B. Mulcahy, J. K. Mitchell, Y. Meirovitch, D. R. Berger, Y. Wu, Y. Liu, W. X. Koh, R. Parvathala, D. Holmyard, R. L. Schalek, N. Shavit, A. D. Chisholm, J. W. Lichtman, A. D. T. Samuel, M. Zhen, Connectomes across development reveal principles of brain maturation. *Nature* **596**, 257–261 (2021).

57. J. E. Richmond, W. S. Davis, E. M. Jorgensen, UNC-13 is required for synaptic vesicle fusion in *C. elegans*. *Nat. Neurosci.* **2**, 959–964 (1999).

58. H. Sass, Sensory encoding of odor stimuli in *Periplaneta americana*. *J. Comp. Physiol. A Neuroethol. Sens. Neural Behav. Physiol.* **107**, 49–65 (1976).

59. M. Meister, T. Bonhoeffer, Tuning and topography in an odor map on the rat olfactory bulb. *J. Neurosci.* **21**, 1351–1360 (2001).

60. H. Saito, Q. Chi, H. Zhuang, H. Matsunami, J. D. Mainland, Odor coding by a mammalian receptor repertoire. *Sci. Signal.*, **2**, ra9 (2009).

61. D. Zwicker, A. Murugan, M. P. Brenner. Receptor arrays optimized for natural odor statistics. *Proc. Natl. Acad. Sci. U.S.A.* **113**, 5570–5575 (2016).

62. S. Qin, Q. Li, C. Tang, Y Tu, Optimal compressed sensing strategies for an array of nonlinear olfactory receptor neurons with and without spontaneous activity. *Proc. Natl. Acad. Sci. U.S.A.* **116**, 20286–20295 (2019).

63. K. Kajiya, K. Inaki, M. Tanaka, T. Haga, H. Kataoka, K. Touhara, Molecular bases of odor discrimination: Reconstitution of olfactory receptors that recognize overlapping sets of odorants. *J. Neurosci.*, **21**, 6018–6025 (2001).

64. H. Spors, M. Wachowiak, L. B. Cohen, R. W. Friedrich, Temporal dynamics and latency patterns of receptor neuron input to the olfactory bulb. *J. Neurosci.* **26**, 1247–1259 (2006).

65. T. Wakabayashi, I. Kitagawa, R. Shingai, Neurons regulating the duration of forward locomotion in *Caenorhabditis elegans*. *Neurosci. Res.*, **50**, 103–111 (2004)..

66. P. A. Garrity, M. B. Goodman, A. D. Samuel, P. Sengupta, Running hot and cold: Behavioral strategies, neural circuits, and the molecular machinery for thermotaxis in C. *elegans* and *Drosophila*. *Genes Dev.*, **24**, 2365–2382 (2010).

67. H. S. Kaplan, M. Zimmer, Brain-wide representations of ongoing behavior: A universal principle? *Curr. Opin. Neurobiol.* **64**, 60–69 (2020).

68. A. Lin, D. Witvliet, L. Hernandez-Nunez, S. W. Linderman, A. D. T. Samuel, V. Venkatachalam, Imaging whole-brain activity to understand behaviour *Nat. Rev. Phys.*, **4**, 292–305 (2022).

69. M. Meister. On the dimensionality of odor space. *eLife*, **4**, e07865 2015).

70. C. Bushdid, M. O. Magnasco, L. B. Vosshall, A. Keller, Humans can discriminate more than 1 trillion olfactory stimuli. *Science* **343**, 1370–1372 (2014).

71. C. D. Wilson, G. O. Serrano, A. A. Koulakov, D. Rinberg, A primacy code for odor identity. *Nat. Commun.* **8**, 1477 (2017).

72. D. R. Albrecht, C. I. Bargmann, High-content behavioral analysis of *Caenorhabditis elegans* in precise spatiotemporal chemical environments. *Nat. Methods* **8**, 599–605 (2011).

73. J. P. Nguyen, A. N. Linder, G. S. Plummer, J. W. Shaevitz, A. M. Leifer. Automatically tracking neurons in a moving and deforming brain. *PLOS Comput. Biol.*, **13**, e1005517 (2017).

74. V. Venkatachalam, N. Ji, X. Wang, C. Clark, J. K. Mitchell, M. Klein, C. J. Tabone, J. Florman, H. Ji, J. Greenwood, A. D. Chisholm, J. Srinivasan, M. Alkema, M. Zhen, A. D. T. Samuel, Pan-neuronal imaging in roaming *Caenorhabditis elegans*. *Proc. Natl. Acad. Sci. U.S.A.* **113**, E1082–E1088.

75. K. M. Hallinen, R. Dempsey, M. Scholz, X. Yu, A. Linder, F. Randi, A. K. Sharma, J. W. Shaevitz, A. M. Leifer. Decoding locomotion from population neural activity in moving *C. elegans*. *eLife*, **10**, e66135 (2021).

76. J. D Storey. A direct approach to false discovery rates. *J. R. Stat. Soc. B* **64**:479–498, 2002.

77. E. Candès, B. Recht. Exact matrix completion via convex optimization. *Commun. ACM*, **55**, 111–119, (2012).

78. L. T. Nguyen, J. Kim, B. Shim, Low-rank matrix completion: A contemporary survey. *IEEE Access* **7**, 94215–94237 (2019).

79. J. Fan, L. Ding, Y. Chen, M. Udell. Factor group-sparse regularization for efficient low-rank matrix recovery. *Adv. Neural Inf. Process. Syst.* **32** (2019).

80. M. Linkert, C. T. Rueden, C. Allan, J. M. Burel, W. Moore, A. Patterson, B. Loranger, J. Moore, C. Neves, D. M. Donald, A. Tarkowska, C. Sticco, E. Hill, M. Rossner, K. W. Eliceiri, J. R. Swedlow, Metadata matters: Access to image data in the real world. *J. Cell Biol.* **189**, 777–782 (2010).

81. P. Kovesi, Good colour maps: How to design them. arXiv:1509.03700 [cs.GR] (12 September 2015).